

Satellite versus ground-based estimates of burned area: A comparison between MODIS based burned area and fire agency reports over North America in 2007

The Anthropocene Review

1–17

© The Author(s) 2015

Reprints and permissions:

sagepub.co.uk/journalsPermissions.nav

DOI: 10.1177/2053019615588790

anr.sagepub.com



**Stéphane Mangeon,^{1,2} Robert Field,²
Michael Fromm,³ Charles McHugh⁴ and
Apostolos Voulgarakis¹**

Abstract

North American wildfire management teams routinely assess burned area on site during firefighting campaigns; meanwhile, satellite observations provide systematic and global burned-area data. Here we compare satellite and ground-based daily burned area for wildfire events for selected large fires across North America in 2007 on daily timescales. In a sample of 26 fires across North America, we found the Global Fire Emissions Database Version 4 (GFED4) estimated about 80% of the burned area logged in ground-based Incident Status Summary (ICS-209) over 8-day analysis windows. Linear regression analysis found a slope between GFED and ICS-209 of 0.67 (with $R = 0.96$). The agreement between these data sets was found to degrade at short timescales (from $R = 0.81$ for 4-day to $R = 0.55$ for 2-day). Furthermore, during large burning days (> 3000 ha) GFED4 typically estimates half of the burned area logged in the ICS-209 estimates.

Keywords

daily burned area, GFED, fire agency, ICS-209, North America, satellite observation

Introduction

Fires are a central component of the Earth system, interacting closely with the atmosphere, the biosphere and humans (Bowman et al., 2009). Global burned-area varies from year to year, e.g. between 1997 and 2011 the satellite estimation we use in this study had a range from 301 to 377

¹Imperial College London, UK

²NASA GISS and Columbia University, USA

³Naval Research Laboratory, USA

⁴US Forest Service, USA

Corresponding author:

Stéphane Mangeon, Space and Atmospheric Physics Group, Department of Physics, Imperial College London, South Kensington Campus, London SW7 2AZ, UK.

Email: stephane.mangeon12@imperial.ac.uk

Mha (Giglio et al., 2013); such information is valuable for understanding the changing role of fires in the Earth system, both globally and regionally. Humans are able to influence otherwise natural fire activity through land management, and fire ignition as well as suppression (Bowman et al., 2011). On longer timescales, humans are able to drive changes in fire activity through influencing climate, because temperature, humidity and precipitation are known to be major drivers of fire occurrence (Pechony and Shindell, 2010). Furthermore, Bistinas et al. (2014) showed global fire frequency is correlated with land use, vegetation type and meteorological factors (dry days, soil moisture and maximum temperature), while human presence tends to noticeably reduce fire activity.

Emissions from fires impact air quality, health and climate forcing on short timescales (Marlier et al., 2013, 2014), while also influencing the longer-term average state of the atmosphere through, for instance, the radiative forcing resulting from biomass-burning greenhouse gases and aerosols (Ward et al., 2012). Our ability to forecast and model air quality and climate impacts of biomass-burning emissions is improving, but is inevitably limited by the accuracy of emissions inputs. Biomass-burning emissions are commonly generated through bottom-up approaches, whereby initial satellite observations of burned area are coupled with vegetation modeling to estimate the amount of dry-matter burned and subsequently emitted (e.g. van der Werf et al., 2006). Therefore to improve emission estimates one can improve the vegetation modeling aspect, and/or the accuracy of the satellite burned-area observations. We investigate the latter.

Remote observation tools for firefighting were first devised in the 1960s (Wilson, 1966), the 3–6 μm infrared (IR) windows were recommended for fire detection. A number of ground- and air-based tools were thus developed (and are still in use by firefighting forces) utilizing IR cameras, such as airplane (or fixed-wing) IR mapping. The jump into the satellite era made fire-detection systematic and global. Today, the Moderate-Resolution Imaging Spectroradiometer (MODIS) is commonly used for its active-fire products (Justice et al., 2002) and burned-area estimates (Giglio et al., 2013). Utilizing burned-area observations, biomass-burning emission databases estimated monthly means (van der Werf et al., 2006) and extended these to daily and sub-daily resolutions using active-fire products (Mu et al., 2011). A comprehensive comparison of emission estimates for North America is available in French et al. (2011).

Space-based estimates provide the only means of estimating emission pulses consistently on a global scale. Assessments of these estimates is typically done in aggregate over large domains and monthly or annual time periods (Giglio, 2007). However, daily or sub-daily estimates are a minimum requirement for modeling the fate of emission pulses, given that meteorological parameters affecting the fate of emissions (e.g. precipitation, wind or atmospheric stability) can vary greatly in the course of a single day. To that end, we compare daily GFED burned-area used in emission estimates against ground-based Incident Status Summary (ICS-209) reports, which for a subset of large wildfires provide daily fire progression estimates for the continental USA. This daily resolution is the shortest timescale available for such systematic comparison.

North America is, arguably, the largest fire-prone domain where such reports are systematically collected. Aside from facilitating emissions estimates, accurate knowledge of burned area in North America is crucial from an economic standpoint: in 2014, the USA's Forest Service spent more than 40% of its total budget on fire suppression (USDA, 2014). An accurate satellite estimation of burned area has the potential to improve forest firefighting efforts and resource deployment, with particular impact on regions with frequent wildland fires but small firefighting presence (e.g. remote areas of Canada). Furthermore, burned area is an indicator of changes in fire regime under changing land-use and climate conditions (Flannigan et al., 2009).

This work aims to support ongoing modeling work to improve the understanding of the fate, emissions and impacts of biomass burning (Marlier et al., 2014) focusing on the injection of plumes from fires into the stratosphere through short-lived, explosive fires (Fromm et al., 2010), with the aim to eventually include these injections within a climate model. However, our results are also applicable to other studies relying on burned-area from satellite observations, in particular for large wildfires.

Data and methods

We compare GFED burned area (agglomerated from the MCD64A1 fire product) with US fire-fighting incident reports, for an 8-day window around each fire's peak burning and examine the change in the correlation between the two datasets for progressively shorter timescales. As an introduction to the study and the nature of the phenomenon investigated, we provide detailed case studies for three fires.

The GFED4 burned area product

The GFED burned area product is obtained from MODIS satellite observations (Giglio et al., 2013). The GFED4 burned area uses the MODIS direct broadcast 500 m collection 5.1 (MCD64A1), which is produced globally using a burned area mapping algorithm (Giglio et al., 2009). This algorithm makes use of the 500 m MODIS imagery coupled with 1 km MODIS active-fire observations from both the Terra and Aqua satellites (which provide hotspots, i.e. locations whose thermal signature suggests a fire). The algorithm obtains burn scars from the imagery through changes in a burn-sensitive vegetation index (which measures changes in the reflectance of the 1.2 μm and 2.1 μm regions of the MODIS sensor). The active-fire observations are then utilized to 'train' the algorithm, because fire hotspots are more detectable than burn scars. Accurate detection is limited to fires above 120 ha, which should pose no issue in our study focusing on large fires. The MCD64A1 products are then aggregated to create the burned-area grids used in GFED4, with size 0.25 degrees in both longitude and latitude.

The GFED4 product was originally designed to produce monthly estimates of burned area and biomass-burning emissions, but is now available at 8-day and daily resolution (<http://www.globalfiredata.org/data.html>; Giglio et al., 2013).

ICS-209 reports

The ICS-209 (http://fam.nwcg.gov/fam-web/hist_209/report_list_209) program is a US National Fire and Aviation Management Web Application that is used to report incident-specific information on more than 40 items such as area burned, percent contained, number of personnel assigned and costs to date (USDA-USDOJ, 2014). This program is used to report large wildfires and any other significant events (e.g. hurricanes, floods or other disasters) on lands under federal protection or federal ownership. The ICS-209 is submitted daily for fire incidents and can provide a synopsis of the wildland fire situation nationally for specific significant incidents. An ICS-209 is required for fire incidents larger than 40 ha in timber fuel types and 120 ha in grass or brush fuel types, or when a dedicated Incident Management Team (IMT) is assigned (USDA-USDOJ, 2014). Although it only focuses on relatively large fires (Short, 2014), it is the only easily accessible dataset that tracks incident information on a daily basis.

ICS-209 have been used to compare burned-area estimates against MODIS fire pixels (Pouliot et al., 2008), to develop a generalized linear mixed-model of containment probability for individual fires (Finney et al., 2009) and to assist in the development of a spatial database of wildland fires in the USA (Short, 2014).

In our analysis, we use the daily burned-area from the ICS-209 reports. This area is estimated by the local incident management organization using a variety of methods, including helicopter Global Positioning Systems (GPS), ground-based reconnaissance and airplane IR mapping. Early on in an incident these numbers are often only the ‘best-guess’ estimate of burned area, with the accuracy improving over the duration of an incident as more accurate mapping techniques are used (airplane IR mapping being the ideal tool with a detailed image and distinct IR fire signature). Multiple fires within close proximity are often grouped into complexes to facilitate their management (and so is their burned-area).

In this study we also used the USGS perimeter data (GeoMAC; <http://rmgsc.cr.usgs.gov/outgoing/GeoMAC/>) to associate GFED pixels with known fires. The perimeter data represents what the IMT considers the fire burn area perimeter. They can be produced daily, or every couple days depending on fire activity and spread. This temporal inconsistency was particularly apparent in the 2007 fires we focused on, with not enough daily information in the USGS perimeter data for systematic daily analysis.

Although not used here, the Monitoring Trends in Burn Severity (MTBS; <http://mtbs.gov/>) project (Eidenshink et al., 2007) provide detailed burn severity maps (once per fire from pre- and post-fire Landsat satellite images). Urbanski et al. (2011) and Morton et al. (2013) used this data set in conjunction with satellite observations for their respective studies.

Case studies of individual fires in the 2007 fire season

We focus on fires that might have caused pyro-cumulonimbus events. The method which we use to choose these fires (summarized below) was detailed and devised in previous studies (e.g. Fromm et al., 2010; Guan et al., 2010). To detect these pyro-cumulonimbus events we use the Ozone Monitoring Instrument (OMI) aerosol observations (which focuses on upper-troposphere, lower-stratosphere particles); if a high-altitude smoke plume is observed with an Aerosol Index (AI; Torres et al., 1998) above 4.0, we ran 24-hour back trajectories from the OMI enhancements using the Hybrid Single-Particle Lagrangian Integrated Trajectory (HYSPPLIT) Model (Draxler and Hess, 1998), with NCEP-NCAR Reanalysis meteorological fields (Kalnay et al., 1996). Separate sets of trajectories were initialized over three distinct vertical levels (3.5–4.5 km, 6.5–7.5 km, 10.5–11.5 km) to capture the range of possible injection heights (Guan et al., 2010). Thus we obtain a range of potential sources for this aerosol plume along the back trajectories paths. Using the USGS perimeter data and GFED we attempt to find a fire that had been intensely burning along this burn trajectory. Once such a fire was identified we carried further investigation on its progression. The full data set containing fire identification, location and daily progression is included as supplementary material (available online).

To illustrate the variety of data available we present detailed case studies for three of the identified fires: The Milford Flat, Ham Lake and Meriwether fires (Figure 1). The Milford Flat fire was the largest distinct fire of the 2007 fire season, the Ham Lake fire was the earliest fire to produce a distinct pyro-cumulonimbus, it also crossed the USA–Canada border; the Meriwether fire is analogous to many other large fires burning in the Northwestern USA in size.

These case studies illustrate the day-to-day evolution of fires in the GFED burned-area product and the MODIS hotspots distributed hourly (using local time in the raw MCD14DL data and without further processing). Notice the variable y-scale between Figures 3, 5 and 6, as the magnitude mattered less than the burn timing in this section of our work. We note that the agency data was

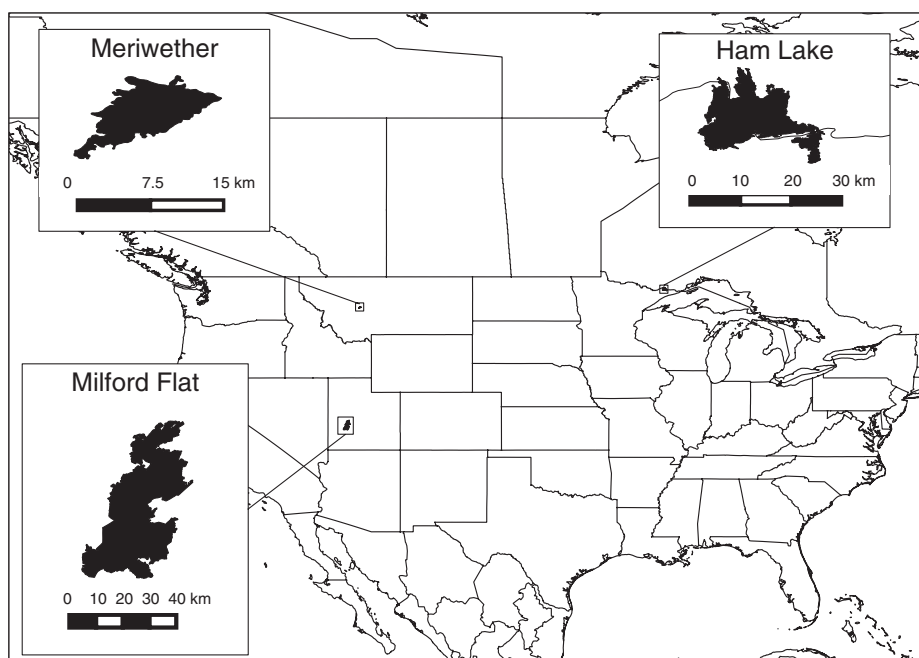


Figure 1. Location of the three case studies within the continental USA. The largest fire observed was the Milford Flat in southern Utah. The Ham Lake is peculiar because of its location as it crossed the Canada–USA border. It led to the first plume observed of the season, at the start of May. The Meriwether fire was a distinguishable pyro-cumulonimbus source within a region that saw extreme burning in the 2007 fire season.

logged on independent local times (at 16:00 h UTC-6 for the Ham Lake fire, 18:00 h UTC-7 for the Milford Flat and Meriwether fires), while GFED represents the burned area for the whole day (UTC). In addition, we show contextual information for each fire.

Contextual information for the pyro-convective phase of each case study is provided by multi-spectral image data from Geostationary Operational Environmental Satellite (GOES). GOES 12 (GOES East) is used for Ham Lake (section ‘Ham Lake’); GOES 11 (GOES West) for Meriwether and Milford Flat. GOES observations are available on a sub-hourly timescale. Animations highlighting the ejection of pyro-cumulonimbus are available as supplementary material and were created with a methodology similar to Fromm et al. (2010) using NOAA’s climate and weather toolkit (Ansari et al., 2010).

We then extend our analysis to the full fire season in 2007, to compare the GFED and agency reported burned area for a representative set of large fires and obtain quantitatively significant results. We pay particular attention to how agreement between GFED and the ICS-209 changed with higher temporal resolution.

Results

We identified a total of 30 candidate pyrogenic aerosol plumes over the USA and 21 over Canada during the 2007 fire season. Back trajectories showed most of these plumes originated from fires in the USA. The northwestern USA experienced intense forest fires in 2007 (Morton et al., 2013).

As a result, there were multiple concurrent fires that were good candidates for the emission of pyro-cumulonimbus. These 51 observed OMI plumes led us to analyze a total of 26 fires. These numbers are not equal as some of the 51 observed aerosol plumes were consecutive plumes (or the same plume observed on consecutive days) from the same fire, hence one fire often led to several observed aerosol plumes. Other plumes in July/August originated from large burning complexes in Idaho and surrounding states (such as the East Zone Complex, the Cascade Complex and the southern Murphy Complex). These fires were often too close together (an issue for satellite observations and GFED) and fell under a single fire management team (their burned area becoming an agglomerate in ICS-209), we could not pinpoint an individual fire as responsible for the observed aerosol plume or distinguish between fires within these neighboring complexes. Therefore these complexes (which likely led to OMI plumes and with characteristically large burned-area) were not included in this study. In an 8-day peak-burning window, the selected fires ranged in size from 3140 to 146,920 ha, with a mean 8-day total of 24,380 ha. This window was centered on the OMI maximum AI detection day attributed to the fire. Unlike other studies we do not investigate final fire size (e.g. Giglio et al., 2006; Urbanski et al., 2011), although for our sample of fires we found that 79.9% of the final burned-area was captured by the ICS-209 within the 8 days investigated.

Individual case studies

Milford Flat. Started by a lightning strike on 6 July 2007, the Milford Flat fire was the largest recorded fire in Utah's history, burning 114,500 ha in its first two days, racing through short grass and sage on 6 July. On 7 and 8 July it spread to the Mineral Mountain Range, where it burned through heavier fuel: brush and pinyon pine-juniper. This shift into woodlands led to the following remarks on fire behavior in the ICS-209: 'Running crown fire, spotting, plume-dominated'. This plume domination coincides with the observation of high concentrations of aerosols by the OMI satellite on 7 July over Utah with an AI of 4.6 and on 8 of July over New Mexico, with an AI of 7.5. Back trajectories of both of these plumes led directly to the Milford Flat fire. The fire was eventually contained after 11 July. GFED4 daily burned-area appears to capture most of the burning of this large fire, as shown by the USGS perimeter data (Figure 2), with some geometrical roughness. (Note: the lowest two grid points with burned area after 9 July are due to the coincidental but distinct Greenville fire.)

According to ICS-209, the Milford Flat fire burned 146,922 ha between 6 and 15 July, GFED shows an accumulated burned-area of 105,465 ha. While this is a good estimate for the total burned-area, the temporal distribution of burning in the GFED product is different from ground observation (Figure 3). While GFED shows a large burned-area on 7 July and a diminution until 13 July, the ICS-209 show two peak-burning days on 7 and 8 July with 62,000 and 52,000 ha burned. The peak observed in the ICS-209 reports on 12 July was in part due to burned-area readjustments after a more accurate mapping by ground crews.

Ham Lake. A major windstorm event in 1999 resulted in the creation of significant fuel loads in the Ham Lake area (Fites et al., 2007). This led to a campaign of fuel reduction in subsequent years to decrease the risks of fire (Fites et al., 2007). Nevertheless, a campfire on 5 May 2007 escaped and the resulting wildfire burned 30,000 ha over its lifetime, with nearly half of the burned area occurring in Canada (as the management team was coordinated between Canadian and American agencies we could study the fire within the ICS-209). Dead leaves, dried wetlands and tree trunks (blown down 8 years before) fueled the fire in what would altogether be

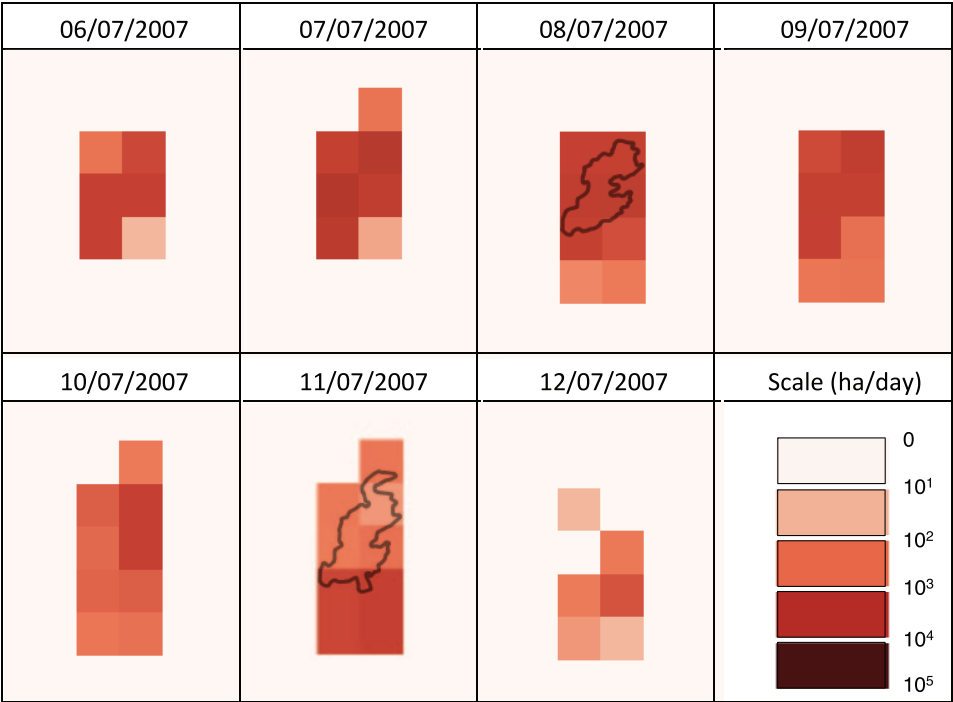


Figure 2. The fire progression of the Milford Flat fire at peak burning between 6 and 12 July 2007. The GFED4 daily burned area product (logarithmic red scale) is overlain with USGS fire perimeters from the forestry services when available, on 8 and 11 July. According to both incident reports and GFED the peak burning occurred on 7 July. Note the southern two grid-boxes represent the coincidental Greenville fire.

classified as boreal forest. When the fire reached areas of standing forest, it would burn as an active crown fire whereby the treetops and leaves are on fire, a characteristic of particularly powerful fires. The fire crossed the border with Canada on 9 May, on 10 May USA/Canada command was unified but the fire spread further east and intensified, leading to pyro-convection. On 14 May, humidity levels above 70% allowed suppression efforts to progress and on 24 May the fire was declared contained after having burned 30,000 ha and costing US\$10.7 million. The burn severity was lower in areas that had undergone prescribed fires to reduce fuel load post-1999 (Fites et al., 2007).

GOES-12 (East) imagery (Figure 4) shows the formation of a pyro-cumulonimbus between 18:00 h and 20:00 h GMT on 10 May. The pyro-convective cloud is gray in the visible (4a), colder than ice-nucleating thresholds (4b), and abnormally warm in the shortwave IR (4c). These thermal properties follow from smoke-modified cloud microphysics (Fromm et al., 2005). Animations of these three spectral views for all three cases are contained in the supplementary material (available online). In the OMI data this fire led to an AI of 14 over Lake Ontario on 11 May. Smoke traceable to the Ham Lake fire was observed on 11 May at 10 km altitude by NASA's Cloud-Aerosol Lidar and Infrared Pathfinder Satellite Observation (CALIPSO) instrument over New York State (http://www-calipso.larc.nasa.gov/products/lidar/browse_images/production/).

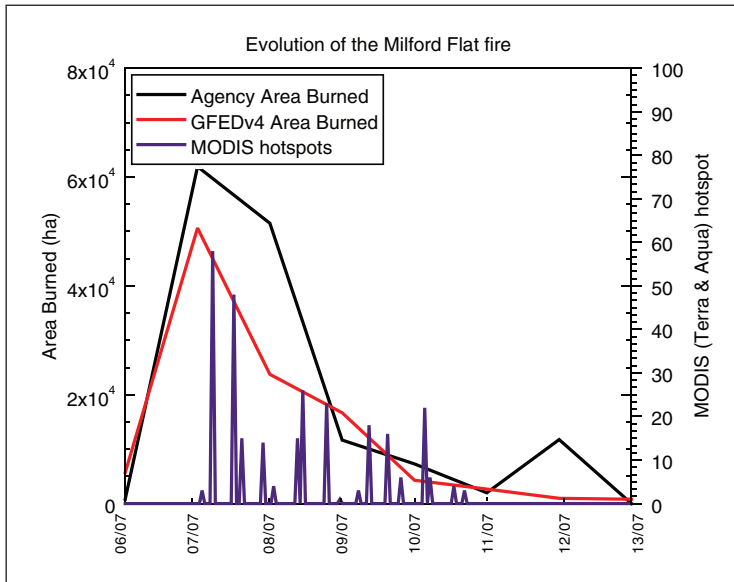


Figure 3. The evolution of the Milford Flat fire, starting on 6 July 2007 until 15 July. Peak burning occurred on 7 July. On the same day a pyro-cumulonimbus was observed and led to a large aerosol plume released that was observed on 7 July and again on 8 July after atmospheric transport. The agency burned area (ha) was derived from the ICS-209 reports. The GFED burned area was obtained by accumulating the grid-boxes within the fire perimeter. The MODIS hotspots are taken hourly from the MCD14MML product from both Terra and Aqua satellites.

The Ham Lake fire progression is characterized by two surges, on 11 and 14 May and a large spread on its first day as shown in Figure 5. Both ICS-209 and GFED burned area capture this timing, although the ICS-209 reports a much stronger peak burning. Over the 8-day analysis window, ICS-209 shows a total burned-area of 27,300 ha compared with 14,700 ha for the GFED burned area.

Meriwether. Sparked by a lightning strike on 21 July 2007, the Meriwether fire in Montana burned 17,500 ha over its lifetime and was declared extinguished at the start of October. The fuel was composed of timber, grass and shrub understory. The fire was particularly difficult to combat because of steep rugged terrain. The Meriwether fire ground crews observed on 28 July: ‘Spectacular plume domination on the north and north east side of the fire’. This was echoed the following day: ‘Spectacular plume domination on the north and north east side of the fire again today’. Such remarks by fire management teams help us pinpoint which fire led to the formation of a pyro-cumulonimbus, since numerous fires were coincidentally burning in this area, see <http://earthobservatory.nasa.gov/NaturalHazards/view.php?id=18820> for a true color MODIS representation of the burning. Large amounts of aerosols were observed on 30 July over Montana and Alberta, with a maximum AI of 8.6, and again on 1 August over Minnesota (7.6 AI). These could both be associated with large fire activities in and around Idaho including the Meriwether fire; it is also probable multiple pyro-cumulonimbus were released from multiple fires.

The fire gradually increased its burning rate, which then dropped on 2 August before exploding again on 3 August (Figure 6). That day’s ICS-209 highlights an intensification of fire activity: ‘Rapid rates of spread in grassy fuels and long range spotting [...] Around 1600 the fire

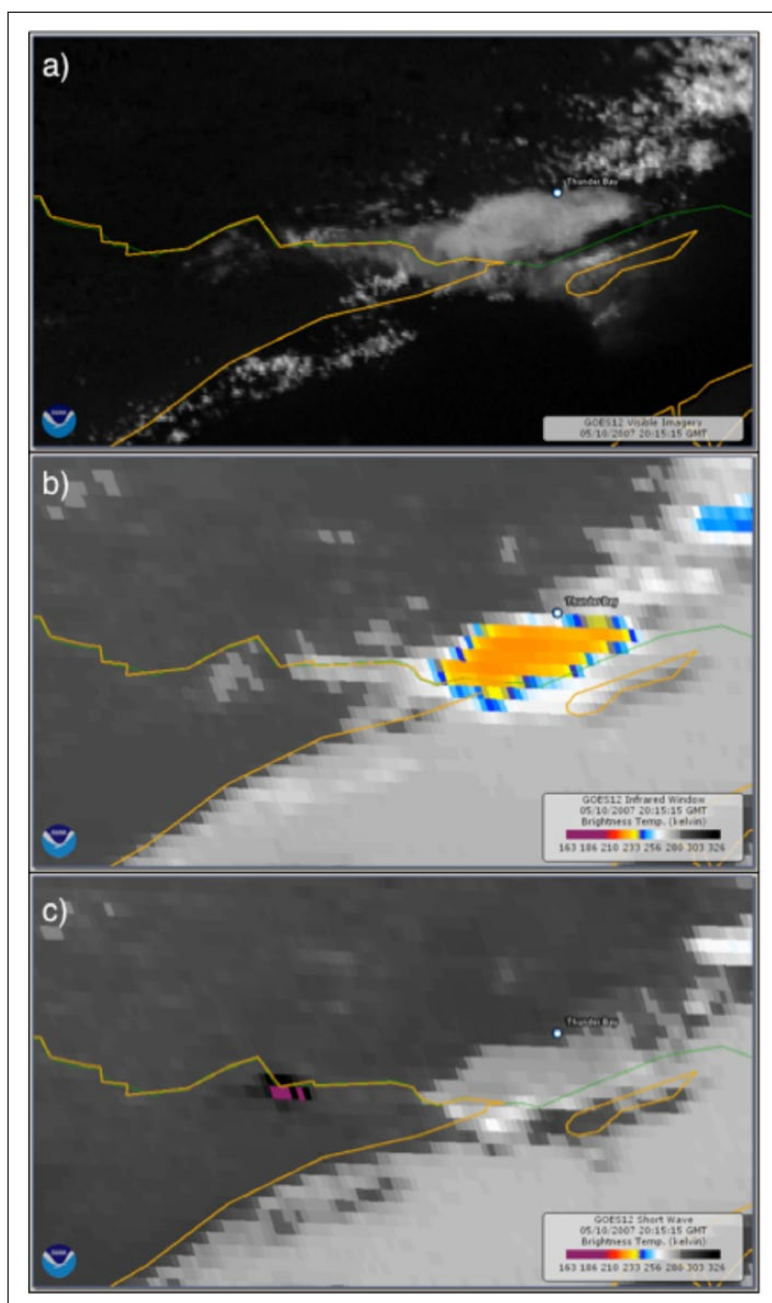


Figure 4. GOES East images of a mature pyro-cumulonimbus generated by the Ham Lake fire on the Minnesota/Ontario border. Image date, time: 10 May 2007, 20:15 UTC. (a) visible, (b) 11 μm cloud-top temperature, (c) 3.9 μm cloud-top temperature. The Ham Lake fire is evident in the 3.9 μm (c) hotspots, which are black or purple (heat saturated; fill value). The pyro-cumulonimbus cloud is gray in the visible (a), colder than ice-nucleating thresholds (b), and abnormally warm in the shortwave IR (c), this is due to smoke-modified cloud microphysics (Fromm et al., 2005).

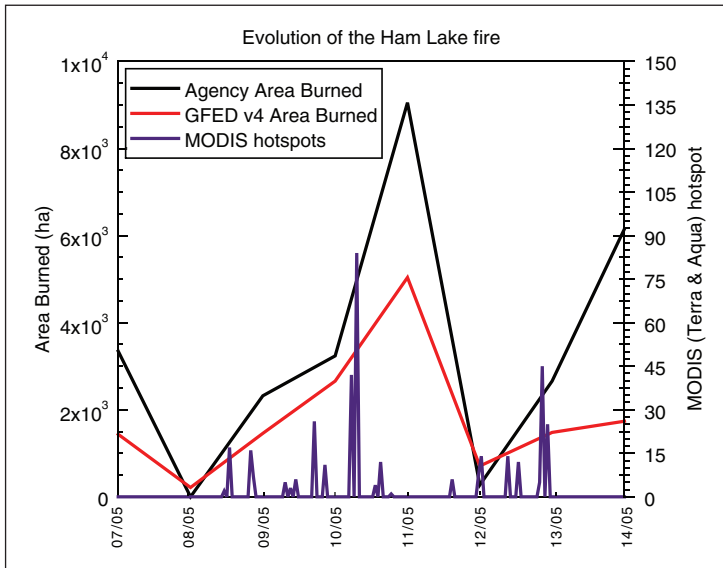


Figure 5. The evolution of the Ham Lake fire from 7 to 14 May 2007. On 10 May it released a major pyro-cumulonimbus that was observed during its travel above the Atlantic. The Ham Lake fire was the first major pyro-convective event of the season and crossed the Canadian border. The agency burned area (ha) was derived from the ICS-209. The GFED burned area was obtained by accumulating the grid-boxes within the fire perimeter. The MODIS hotspots are taken hourly from the MCD14ML product from both Terra and Aqua satellites.

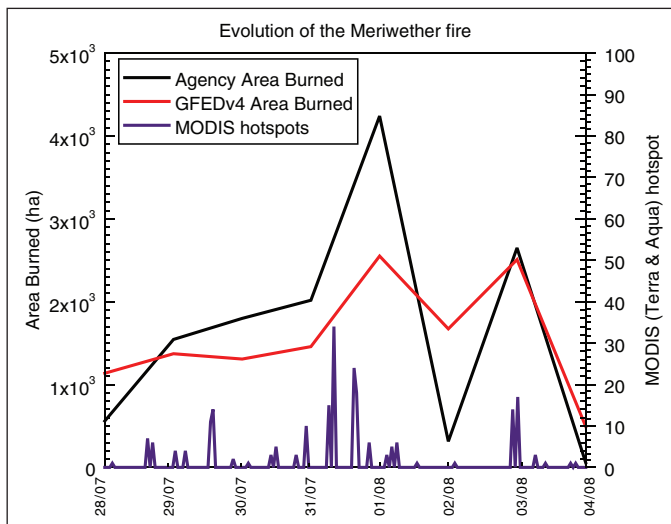


Figure 6. Progression of the Meriwether fire, from 28 July until 4 August. This fire was the smallest case study but stood out because of the remarks included in the incident reports. GFED captures the double peak observed on 1 and 3 July, in a more uniform burning than incident reports and MODIS hotspots suggest. The agency burned area (ha) was derived from the ICS-209. The GFED burned area was obtained by accumulating the grid-boxes within the fire perimeter. The MODIS hotspots are taken hourly from the MCD14ML product from both Terra and Aqua satellites.

spotted across the line'. Both GFED and ICS-209 predict a burned area close to 13,000 ha over the 8-day window investigated, with two peaks of daily burned-area on 1 and 3 August. Nevertheless, satellite observations appear to produce a smoother burned-area distribution than ICS-209.

Throughout these three case studies we have illustrated the breadth of specific information available for individual wildfires and the methodology that was used subsequently for all 26 fires studied in the 2007 fire season. GOES imagery showed that pyro-cumulonimbus formation is a frequent and observed phenomenon linked to North American wildfires. We found that while days of large burning were observed at similar times in both GFED4 and ICS-209, peaks in burned area were sharper and higher in ICS-209; we next focus on quantifying this observation with a larger sample.

The 2007 fire season

We carried out investigations of 26 fires representing the 2007 fire season, starting with the Ham Lake fire on 5 May and ending with the Californian Butler 2 fire on 22 September. Although some fires were still burning in North America this corresponds to the last plume observed in the OMI data. The GFED4 estimates of burned area, over the whole fire season and across most fire sizes, are lower than those from ICS-209 (Figure 7). Nevertheless, there is a strong ($R = 0.96$) linear relationship between agency and GFED burned area, with a slope of 0.67. This low GFED bias is consistent with other studies which used yearly, aggregated agency statistics from North America (Giglio et al., 2006; Ruiz et al., 2014). Our selected fire sizes fell roughly into two clusters: 23 fires that were less than 30,000 ha and three larger fires that were 147,000 ha (Milford Flat, Utah), 80,000 ha (Winecup Complex, Oregon) and 60,000 ha (Old Fort, Alberta). The paucity of fires greater than 30,000 ha likely reflects our omitting the Murphy Complex fires and other large complexes. For the cluster of fires burning less than 30,000 ha we found a slope of 0.74 and $R = 0.92$ (by omitting the larger fires we attempt to avoid their overrepresentation in a linear regression). This suggests a systematic tendency of GFED4 to underestimate burned area compared with ICS-209 ground estimates.

To investigate the reliability of the GFED burned area product at the shorter timescales required for accurate modeling of emission pulses, we compared agreement with ICS-209 data set at different temporal resolutions, ranging from 8 days to 1 day (Table 1). We do not include the three largest fires in this analysis, as the quality of the ICS-209 reporting was poorer for the Old Fort and Winecup fires. Inclusion of these three large fires does not qualitatively affect our figures, although it has a quantitative impact.

The agreement between GFED and ICS-209 estimates of burned area for an 8-day window is strong ($R = 0.92$). This relationship slightly decreases ($R = 0.81$) for 4-day windows. The correlations are further weakened when considering 2-day windows, ranging from $R = 0.21$ to $R = 0.83$. The correlations are generally low for individual days, except for the first day of burning (0.82). Across the 26 fires investigated, GFED and incident reports agreed on 54% of peak-burning dates, with GFED finding 55% of the burned area declared by incident reports on those peak-burning days.

Discussion

Our linear regression analysis found a slope of 0.67 between GFED and ICS-209 burned-area (with $R = 0.96$). Supporting this finding, Ruiz et al. (2014), using annual and regional fire statistics (from

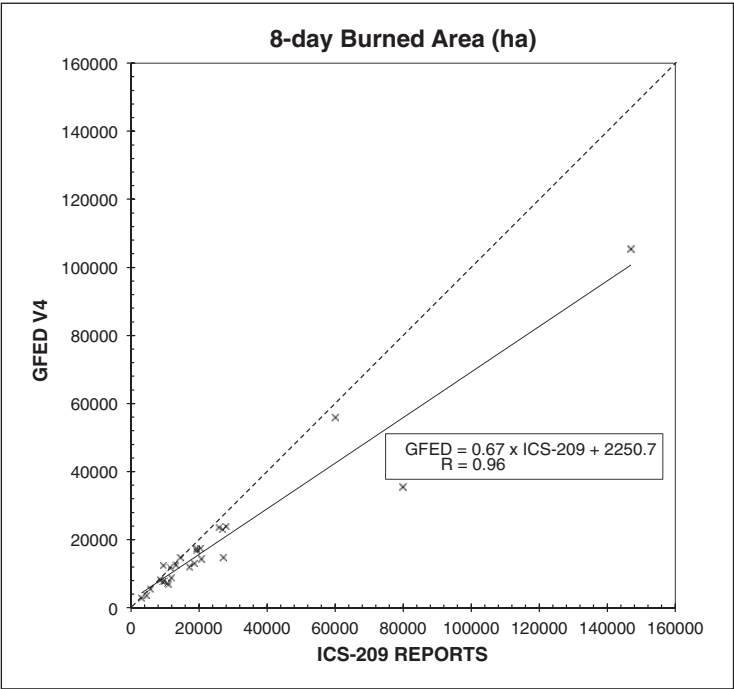


Figure 7. Scatterplot of area burned within an 8-day window for 25 fires during the 2007 fire season in North America. GFED v4 is a satellite-based, MODIS-derived (MCD64A1), burned area product, and the ICS-209 reports are incident-specific reports filled by incident management teams for resource allocation. We find a 67% slope between the data sets and a Pearson coefficient $R = 0.96$. Note the definition of total area burned differs with datasets: GFEDv4 represents it as the surface scorched while the ICS-209 report the area contained within the observed fire perimeter. In effect this is relevant for unburned islands and water/barren surfaces within the fire perimeter.

Table 1. Sensitivity to temporal resolution of the agreement between GFEDv4 burned area and ICS-209 incident reports represented by the Pearson coefficient (R). While the 8-day and 4-day aggregates strongly agree, the two data sets become less comparable at a smaller timestep, this is particularly true of the late stages.

| Time window | 1 | 2 | 3 | 4 | 5 | 6 | 7 | 8 |
|-------------|------|-----|------|------|------|------|------|------|
| 8 day | 0.92 | | | | | | | |
| 4 day | 0.82 | | | | 0.81 | | | |
| 2 day | 0.53 | | 0.62 | | 0.83 | | 0.21 | |
| 1 day | 0.82 | 0.4 | 0.47 | 0.27 | 0.58 | 0.58 | 0.32 | 0.29 |

the Alaska Fire Service and the Canadian Forest Service National Fire Database) as reference data, found that across a variety of burned area products, the MCD64A1 (i.e. the MODIS data used in GFED) produced the best correlation with the reference data amongst other burned area products. They also found that MCD64A1 underestimates burned area for the years 2001–2011 (slope of

0.76) but with a very high linear relationship ($R^2 = 0.84$), consistent with our results. Randerson et al. (2012) suggested small fires could account for some of this discrepancy in aggregate statistics; this should not apply to our sample of individual large fire events. Meanwhile, Soja et al. (2009) considered the difference in burned area estimates from MODIS and GOES in the context of air quality assessments, using the Western Regional Air Planning Association (WRAP) data sets of ground data for Oregon and Arizona. Even though their burned area assessment is based on associating a constant burned area to each fire hotspot and therefore different from GFED4, they do find large fires to be 30% (Oregon) and 5% (Arizona) above the MODIS-derived burned area, similar to our findings for GFED4.

We also observe that the peak-burning day is coincident in both ICS-209 and GFED4 for 15 out of 26 fires. For the remaining 11 fires the peak-burning day was off by an average of 1.63 days, a figure consistent with GFED4's own burn date uncertainty (Giglio et al., 2013). We also noticed GFED4 associated peak burning with a later date than ICS-209 for 8 out of those 11 fires. On that peak-burning day, we observe GFED predicts 55% of the burned area logged in the ICS-209, which hints that GFED4 might be underestimating burned area on days of large burning. To explore this we identified 56 days when more than 3000 ha were burned according to ICS-209 reports. During those 56 days, GFED estimated 54% of the burned area logged in ICS-209. One potential explanation for this low bias would be that the algorithm used for the MCD64A1 product might discard observations made during extreme burning, when emitted radiation from a fire could be confused with reflected sunlight (it emits within the long-wave reflective bands) (Giglio et al., 2013; Giglio, personal communication, 2014). It is also possible that the pyro-cumulonimbus themselves obscure MODIS observation (and IR) although in our case studies we have observed their release to occur in the late afternoon around 18:00 h local time while MODIS satellites' zenith overpass are at 13:30 h (Aqua) and 22:30 h (Terra) local time; this time difference should dampen the effect obscuration from such clouds might have on observations. Note that GOES imagery was utilized by the Fire Locating and Modeling of Burning Emissions (FLAMBE), operational since 1999 and summarized in Reid et al. (2009), with more frequent observations the potential for pyro-cumulonimbus to obscure observations could be more evident. Finally, there is also a possibility that this bias emerges from ICS-209 burned area itself. To address this uncertainty in both variables we carried out major-axis regression (a statistical technique that accounts for an uncertainty in both x and y , see for example Clarke, 1980). We found our major-axis regression slope of 0.69 between GFED and ICS-209 burned area, supporting our linear regression results.

There are limitations to the data sets we have used: our sample is restricted to fires with a total burned area above 3000 ha; for small fires, Hawbaker et al. (2008) examined satellite detections against fire perimeters and found that less than 50% of fires below 105 ha were detected using both Terra's and Aqua's MODIS instrument. The inclusion of small fires to total burned area was shown by Randerson et al. (2012) to lead to a 35% global increase in burned area compared with GFED. We found 8 out of 26 fires exploded within their first three days (when the bulk of the burned area occurred in the few days following the first agency record of the fire); at this stage ICS-209 burned area might be judged as a best-guess estimate with hastily dispatched, less precise measurement methods. In examining the records, we nevertheless found frequent mentions of accurate airplane IR for three of those within the first days of the analysis. Conversely, the final two days of our 8-day analysis window show strong differences between incident reports and GFED, when MODIS might observe burned area that ground crews will not account for since it is contained within the fire perimeter.

While the ICS-209 data set could be considered to represent a ground truth for satellite burned area products, it is important to bear in mind that strictly speaking it only provides information about the fire perimeter. This is relevant for the unburned island phenomenon, whereby areas contained within the fire perimeter will remain unburned following the passage of a fire. Kolden et al. (2012) observe unburned areas within the fire perimeters constitute up to 30% of the total burned area for fires larger than 10,000 ha within three US national parks.

Although we have found that GFED underestimates burned area compared with ICS-209, other studies have shown that estimates of burned area from satellites can be larger than ground-based estimates. Urbanski et al. (2009), for example, used Burned Area Reflectance Classification (BARC) burn severity maps (Clark et al., 2006) as ground truth to validate their burned area direct broadcast (MODIS-DB) for the western USA. They find their product to overestimate burn area by 56%. Meanwhile a comparison between MODIS burn area and MTBS maps by Giglio et al. (2009) find a 1.12 slope and $R^2 = 0.995$ for the USA across seven fires. These trends are opposite to that we observe, possibly because of inner unburned areas. Using MTBS maps it would be possible to investigate this bias for our sample.

Biomass-burning emissions with high temporal accuracy are crucial for the study of short-lived events such as pyro-cumulonimbus formation. This temporal accuracy is also important for the study of the impacts of emissions on air quality, atmospheric composition and climate (see e.g. Chen et al., 2009; Marlier et al., 2014; Petrenko et al., 2012; Wang and Christopher, 2006; Wang et al., 2006). In this study we highlighted that the agreement between GFED4 burned area and ICS-209 is substantially degraded when the window for comparison is less than 4 days.

The ease of access of the ICS-209 and their coverage provides a capability to obtain first-hand observations of individual fire events for a variety of applications. Moreover, these reports also contain qualitative situation assessment and fuel information that could be used to improve fire modeling and emission estimates (fuel types for fire-behavior models, in situ fire observations and meteorological phenomena for atmospheric interactions). Our study was constrained to the 2007 fire season, but since records date back to 2002 a similar approach could be used to study interannual variability. We expect the use of an ICS-209-derived burned area data set will lead to sharper emission estimates on days of extreme burning.

Conclusion

We have shown GFED4 can reasonably identify the peak day of burning and track the temporal progression of individual fires, such as the Milford Flat, Ham Lake fire and Meriwether fires. However, GFED4 systematically underpredicts the burned area both on peak fire days and overall when compared with ICS-209; GFED registers around half of the ICS-209 burned-area on strong burning days (above 3000 ha per day) and 79% over an 8-day analysis window. The best agreement between the two data sets was found for an 8-day window, an agreement that progressively worsened for shorter time windows. This suggested a potential correction to burned area observed for brief and severe North American fires. However, data sets such as ICS-209 are not available for most regions of the world. Thus, a recognition and quantification of the biases inherent in GFED4 (and similar products) is important given that these products are likely to continue to be the major source of information for estimates of biomass-burning emissions, and that such estimates are required on daily and sub-daily timescales in order to be able to consider the effects of biomass burning on atmospheric chemistry, with implications for longer-term atmospheric composition and climate.

Key acronyms

| | | |
|---------|---|---|
| GFED | Global Fire Emission Data (version 4) | A global, widely used data set for biomass-burning emission |
| ICS-209 | The Incident Status Summary reports | Used by federal agencies to assess ground situation. Logged daily it regroups a variety of information on incident status, including acreage burned |
| MODIS | Moderate-Resolution Imaging Spectroradiometer | A global coverage satellite commonly used to detect fire hotspots and infer burned area |
| MCD64A1 | MODIS burned area product | Derived from surface reflectance changes it provides daily burned area globally |
| GOES | Geostationary Operational Environmental Satellite | A geostationary satellite focusing on America with lower spatial coverage than MODIS but with sub-hourly measurements |
| OMI A1 | Ozone Monitoring Instrument's Aerosol Index | An index that highlights the presence of light-absorbing aerosols. Used in our study to identify pyro-cumulonimbus |

Acknowledgements

We thank Louis Giglio and Guido Van der Werf for their helpful comments and suggestions. We thank Hua Sun in Alberta, Garth Hoeppe in Manitoba as well as Philippe Dion and Francis Barriault in Quebec for providing us with provincial wildfire information. We also thank John Little at the Canadian Forestry Service.

Funding

Funding for this work was provided by the NASA Atmospheric Chemistry Modeling and Analysis Program grant NNX13AK46G. The lead author wishes to thank the European Commission's Marie Curie Actions International Research Staff Exchange Scheme (IRSES) for funding his placement at NASA GISS and Columbia University, and the Natural Environment Research Council (NERC, UK) and the UK Met Office for ongoing financial support.

References

Ansari S, Del Greco S and Hankins B (2010) *The Weather and Climate Toolkit*. AGU Fall Meeting Abstract -1, 06.

Bistinas I, Harrison SP, Prentice IC et al. (2014) Causal relationships versus emergent patterns in the global controls of fire frequency. *Biogeosciences* 11: 5087–5101.

Bowman DMJS, Balch J, Artaxo P et al. (2009) Fire in the Earth system. *Science* 324: 481–484. DOI: 10.1126/science.1163886.

Bowman DMJS, Balch J, Artaxo P et al. (2011) The human dimension of fire regimes on Earth. *Journal of Biogeography* 38: 2223–2236.

Chen Y, Li Q, Randerson JT et al. (2009) The sensitivity of CO and aerosol transport to the temporal and vertical distribution of North American boreal fire emissions. *Atmospheric Chemistry and Physics* 9: 6559–6580.

Clark J, Bobbe T, Wulder M et al. (2006) Using remote sensing to map and monitor fire damage in forest ecosystems. In: M Wilder and S Franklin (eds) *Forest Disturbance and Spatial Patterns, GIS and Remote Sensing Approaches*. Boca Raton, FL: CRC Press, pp. 113–132.

Clarke MRB (1980) The reduced major axis of a bivariate sample. *Biometrika* 67: 441–446.

- Draxler RR and Hess G (1998) An overview of the HYSPLIT_4 modelling system for trajectories. *Australian Meteorological Magazine* 47: 295–308.
- Eidenshink J, Schwind B, Brewer K et al. (2007) A project for monitoring trends in burn severity. *Fire Ecology* 3: 3–21.
- Finney M, Grenfell IC and McHugh CW (2009) Modeling containment of large wildfires using generalized linear mixed-model analysis. *Forest Science* 55: 249–255.
- Fites JA, Reiner A, Campbell M et al. (2007) *Fire Behavior and Effects, Suppression, and Fuel Treatments on the Ham Lake and Cavity Lake Fires*. Superior National Forest, Eastern Region, USDA Forest Service.
- Flannigan MD, Krawchuk MA, de Groot WJ et al. (2009) Implications of changing climate for global wildland fire. *International Journal of Wildland Fire* 18: 483–507.
- French NHF, de Groot WJ, Jenkins LK et al. (2011) Model comparisons for estimating carbon emissions from North American wildland fire. *Journal of Geophysical Research Biogeosciences* 116: G00K05.
- Fromm M, Bevilacqua R, Servranckx R et al. (2005) Pyro-cumulonimbus injection of smoke to the stratosphere: Observations and impact of a super blowup in northwestern Canada on 3–4 August 1998. *Journal of Geophysical Research Atmospheres* 110: D08205.
- Fromm M, Lindsey DT, Servranckx R et al. (2010) The untold story of pyrocumulonimbus. *Bulletin of the American Meteorological Society* 91: 1193–1209.
- Giglio L (2007) Characterization of the tropical diurnal fire cycle using VIRS and MODIS observations. *Remote Sensing of the Environment* 108: 407–421.
- Giglio L, Loboda T, Roy DP et al. (2009) An active-fire based burned area mapping algorithm for the MODIS sensor. *Remote Sensing of the Environment* 113: 408–420.
- Giglio L, Randerson JT and van der Werf GR (2013) Analysis of daily, monthly, and annual burned area using the fourth-generation global fire emissions database (GFED4). *Journal of Geophysical Research Biogeosciences* 118: 317–328.
- Giglio L, van der Werf G, Randerson J et al. (2006) Global estimation of burned area using MODIS active fire observations. *Atmospheric Chemistry and Physics* 6: 957–974.
- Guan H, Esswein R, Lopez J et al. (2010) A multi-decadal history of biomass burning plume heights identified using aerosol index measurements. *Atmospheric Chemistry and Physics* 10: 6461–6469.
- Hawbaker TJ, Radeloff VC, Syphard AD et al. (2008) Detection rates of the MODIS active fire product in the United States. *Remote Sensing of the Environment* 112: 2656–2664.
- Justice CO, Giglio L, Korontzi S et al. (2002) The MODIS fire products. *Remote Sensing of the Environment* 83: 244–262.
- Kalnay E, Kanamitsu M, Kistler R et al. (1996) The NCEP/NCAR 40-year reanalysis project. *Bulletin of the American Meteorological Society* 77: 437–471.
- Kolden CA, Lutz JA, Key CH et al. (2012) Mapped versus actual burned area within wildfire perimeters: Characterizing the unburned. *Forest Ecology and Management* 286: 38–47.
- Marlier ME, DeFries RS, Voulgarakis A et al. (2013) El Nino and health risks from landscape fire emissions in southeast Asia. *Nature Climate Change* 3: 131–136.
- Marlier ME, Voulgarakis A, Shindell DT et al. (2014) The role of temporal evolution in modeling atmospheric emissions from tropical fires. *Atmospheric Environment* 89: 158–168.
- Morton DC, Collatz GJ, Wang D et al. (2013) Satellite-based assessment of climate controls on US burned area. *Biogeosciences* 10: 247–260.
- Mu M, Randerson JT, van der Werf GR et al. (2011) Daily and 3-hourly variability in global fire emissions and consequences for atmospheric model predictions of carbon monoxide. *Journal of Geophysical Research Atmospheres* 116. DOI: 10.1029/2011JD016245.
- Pechony O and Shindell DT (2010) Driving forces of global wildfires over the past millennium and the forthcoming century. *Proceedings of the National Academy of Sciences*. DOI: 10.1073/pnas.1003669107.
- Petrenko M, Kahn R, Chin M et al. (2012) The use of satellite-measured aerosol optical depth to constrain biomass burning emissions source strength in the global model GOCART. *Journal of Geophysical Research Atmospheres* 117: D18212.

- Pouliot G, Pace TG, Roy B et al. (2008) Development of a biomass burning emissions inventory by combining satellite and ground-based information. *Journal of Applied Remote Sensing* 2: 021501–021501–17.
- Randerson JT, Chen Y, van der Werf GR et al. (2012) Global burned area and biomass burning emissions from small fires. *Journal of Geophysical Research Biogeosciences* 117: G04012.
- Reid JS, Hyer EJ, Prins EM et al. (2009) Global monitoring and forecasting of biomass-burning smoke: Description of and lessons from the Fire Locating and Modeling of Burning Emissions (FLAMBE) program. *IEEE Journal of Selected Topics in Applied Earth Observations and Remote Sensing* 2: 144–162.
- Ruiz JAM, Lázaro JRG, Cano I del Á et al. (2014) Burned area mapping in the North American boreal forest using Terra-MODIS LTDR (2001–2011): A comparison with the MCD45A1, MCD64A1 and BA GEOLAND-2 products. *Remote Sensing* 6: 815–840.
- Short KC (2014) A spatial database of wildfires in the United States, 1992–2011. *Earth System Science Data* 6: 1–27.
- Soja AJ, Al-Saadi J, Giglio L et al. (2009) Assessing satellite-based fire data for use in the National Emissions Inventory. *Journal of Applied Remote Sensing* 3: 031504–031504–29.
- Torres O, Bhartia PK, Herman JR et al. (1998) Derivation of aerosol properties from satellite measurements of backscattered ultraviolet radiation: Theoretical basis. *Journal of Geophysical Research Atmospheres* 103: 17,099–17,110.
- Urbanski SP, Hao WM and Nordgren B (2011) The wildland fire emission inventory: Western United States emission estimates and an evaluation of uncertainty. *Atmospheric Chemistry and Physics* 11: 12,973–13,000.
- Urbanski SP, Salmon JM, Nordgren BL et al. (2009) A MODIS direct broadcast algorithm for mapping wildfire burned area in the western United States. *Remote Sensing of the Environment* 113: 2511–2526.
- United States Department of Agriculture (USDA) (2014) *Fiscal Year 2015 Budget Overview*. United States Department of Agriculture Forest Service.
- United States Department of Agriculture-US Department of Interior (USDA-USDOI) (2014) *ICS-209 Program (NIMS) User's Guide*. US Forest Service-US Department of Interior.
- Van der Werf GR, Randerson JT, Giglio L et al. (2006) Interannual variability in global biomass burning emissions from 1997 to 2004. *Atmospheric Chemistry and Physics* 6: 3423–3441.
- Wang J and Christopher SA (2006) Mesoscale modeling of Central American smoke transport to the United States: 2. Smoke radiative impact on regional surface energy budget and boundary layer evolution. *Journal of Geophysical Research Atmospheres* 111: D14S92.
- Wang J, Christopher SA, Nair US et al. (2006) Mesoscale modeling of Central American smoke transport to the United States: 1. ‘Top-down’ assessment of emission strength and diurnal variation impacts. *Journal of Geophysical Research Atmospheres* 111: D05S17.
- Ward DS, Kloster S, Mahowald NM et al. (2012) The changing radiative forcing of fires: Global model estimates for past, present and future. *Atmospheric Chemistry and Physics* 12: 10,857–10,886. DOI: 10.5194/acp-12-10857-2012.
- Wilson RA (1966) The remote surveillance of forest fires. *Applied Optics* 5: 899–904.